Mechanical Properties of Materials for MEMS based Sensor Applications

K. S. S. Eswar Raju[a], Samir V. Kamat*[a], Amita Gupta[b]
[a]Defence Metallurgical Research laboratory, Kanchanbagh, Hyderabad, India 500058
[b]Solid State Physics Laboratory, Timarpur, Delhi 110054

ABSTRACT

Development of commonly used MEMS devices such as vibration sensors, accelerometers pressure sensors involve fabrication of thin membranes, cantilevers and diaphragms. These structures are fabricated using materials such as silica, silicon nitride and other thin films on silicon substrates. It is important to measure the mechanical properties of these materials and films for designing as well as evaluating the performance of MEMS devices. The mechanical properties of these materials are dependent on the length scale and hence these properties cannot be measured using bulk specimens and have to be determined at the same length scale as that used in the actual device. Nanoindentation is by far the most popular technique to measure the mechanical properties at small length scales. In this paper we have briefly described the nanoindentation technique and how it can be used to measure the mechanical properties of these materials. The mechanical behaviour of p-doped <100> silicon was studied using nanoindentation. Silicon was found to undergo stress induced phase transformation underneath the indenter as shown by the observation of pop-out in the unloading curve during a nanoindentation test. The effect of load and loading rate on this phase transformation was also investigated. Mechanical properties of thermally grown silica film on silicon substrate were also measured in this work.

Keywords: Silicon; Nanoindentation; Oliver-Pharr analysis; Hardness; Modulus; Phase Transformation

1. INTRODUCTION

Microelectromechanical systems (MEMS) comprise a class of structures that are poorly characterized in terms of reliability. Many MEMS are designed for long operating lives exploiting their high intrinsic strength and stability. Current MEMS manufacturers naturally wish to maximize the performance of their devices. This may mean pushing the mechanical limits of the device materials. Short-term failure modes can be easily tested by increasing the demands, either electrical or mechanical, placed on the manufactured device. Long term reliability is more problematic given that the demands imposed on devices in proof testing may not reveal long term failure modes.

It is therefore important to define the mechanical limits of these microelectromechanical devices if they are to be intelligently designed and applied. Failure modes, including crack initiation and propagation processes, have to be characterized if we expect their application without first requiring years of reliability data. Environmental effects can both exacerbate failure modes and create new ones. Therefore we cannot apply our knowledge of macro-mechanical properties directly to the properties of MEMS materials. The effects of microstructure and fabrication can also become significant on the micro-scale even when they are irrelevant in larger, macro-scale structures. Hence, it is necessary to characterize the mechanical properties to of MEMS materials at the same length scales as that used in MEMS devices to ensure their long term reliability.

Various methods have been reported by researchers for testing various mechanical properties of MEMS materials such as tensile strength, yield strength, ductility and fracture strength [1-5]. These techniques measure the properties of free-standing films. In recent years, nanoindentation has emerged as a convenient tool in mechanical characterization of materials at small length scales. A gamut of mechanical properties such as hardness, elastic modulus, fracture toughness, fatigue, adhesion strengths, scratch, wear resistance etc can be measured using a nanoindenter [6-10]. The advantage of nanoindentation technique is that no additional specimen preparation is required and mechanical properties can be measures directly on the device. In the present study, we have investigated the mechanical behaviour of p-doped <100> silicon as well as thermally grown silica film on silicon using nanoindentation technique.

* kamat@dmrl.drdo.in; phone 91-40-24566518; Fax 91-40-24340559

2. METHODOLOGY

Nanoindentations were made on standard wafers of <100> p-doped silicon and silica film using a Nanoindenter from CSM Instruments. Silica film is thermally grown on the silicon wafer at 1000°C and is subsequently etched to form the diaphragm as shown in Fig. 1. The thickness of the film is 1 μm. A three-sided pyramidal Berkovich diamond indenter having an included angle of 142.3° between the opposite faces and a radius of curvature of the tip of 150 nm is used for indentation experiments. In the indentation tests done for this study, a simple indentation sequence was followed. The indenter is loaded at a specified rate to a pre-determined load and is held constant for 10 seconds at maximum load, followed by unloading. Indentation tests were done over a range of loads. For the loading rate experiments, a range of loading and unloading rates from 0.5 mN/s to 5 mN/s were used. Matrices of four indents were made at four different regions, each spaced 10 μm apart, for each condition. The surface roughness of the films was also measured using atomic force microscope (AFM) prior to nanoindentation measurements. AFM was also used to image the residual indent to determine the extent of pile-up or sink-in. In the case of silicon, indentations were carried out at peak loads of 15 mN, 25 mN, 50 mN, 75 mN and 100 mN. In the loading rate tests on silicon, loading/unloading rates of 25mN/min, 50mN/min, 100mN/min and 300mN/min are used t approach a peak load of 75 mN. In the case of nanoindentation of silica film indentations were done at peak loads of 1.5 mN, 5 mN and 10 mN. Depth sensing nanoindentation provides the variation of indentation load, P, as a function of indentation penetration depth, h.

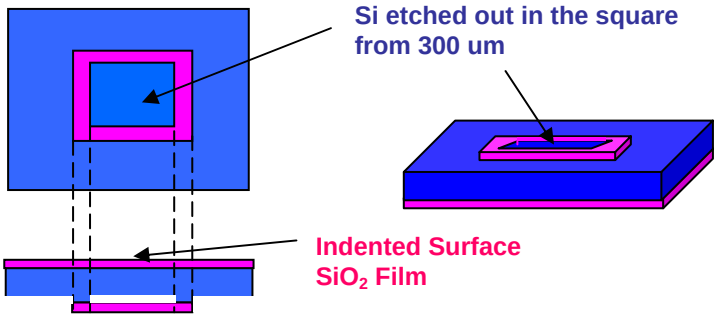

Fig. 1 Silicon etched out from beneath. Silica film on silicon is the indented surface.

The Young's modulus and hardness are calculated from the unloading curve using Oliver and Pharr analysis [11] which uses two basic premises:

(i) the deformation upon unloading is purely elastic;

(ii) the compliance of the sample and the indenter tip can be combined as a system of springs in series, with the effective (or reduced) modulus E_{eff} being

$$\frac{1}{E_{eff}} = \frac{1-\nu_i^{\backslash 2}}{E_i} + \frac{1-\nu_s^{\,2}}{E_s} \tag{1}$$

where E and υ represents the Young's modulus and Poisson's ratio of the indenter, i and sample, s, respectively. The method starts with the fit of the unloading curve to the power–law relation:

$$P = C(h - h_f)^m \tag{2}$$

where C and m are fitting parameters and h and h_f the instantaneous and residual displacements of the indenter. The unloading stiffness S is then obtained by finding the slope at h_{max} by differentiating equation (2) i.e

$$S = mC(h - h_f)^{m-1} \tag{3}$$

The contact depth h_c between the indenter and the specimen can be estimated using

$$h_c = h_{\max} - \varepsilon \frac{P_{\max}}{S} \tag{4}$$

here, P_{max} is the peak load and ε is a constant related to the indenter geometry. Thus, the projected contact area A_c is established by evaluating an empirically determined indenter shape function at the contact depth. Finally, the nano-indentation hardness H_{O-P} and effective elastic modulus E_{eff} are calculated by [11]

$$H_{O-P} = \frac{P_{\max}}{A_c} \tag{5}$$

$$E_{eff} = \frac{\sqrt{\pi}}{2} \frac{S}{\sqrt{A_c}} \tag{6}$$

The elastic modulus of the film can then be calculated from E_{eff} using equation (3), wherein the diamond indenter has a Poisson's ratio of 0.07 and E of 1141 GPa [12].

3. RESULTS AND DISCUSSION

3.1. Silicon:

Figures 2 (a) to (e) show the load-indentation depth curves for p-doped <100> silicon at five different loads. The nature of unloading curve was found to vary with the load. In general, in the unloading portion of the load-indentation depth curves, a pop-out is observed for loads above 25 mN whereas an elbow is observed for loads below 25 mN. For 25 mN load, in some cases a pop-out is seen in the unloading portion of the load-indentation depth plot whereas in other cases an elbow is seen as illustrated in Fig. 2 (d). The load- indentation depth curves at 15 mN have consistently shown elbow in the unloading curve as shown in Fig. 2 (e). It could also be observed that the pop-out does not occur consistently at a particular load during unloading even when the indentations are performed at the same maximum load. However, unlike the pop-out, the elbow bend in the unloading curve occurs consistently at a particular load in the unloading curve. The hardness and elastic modulus are obtained using Oliver and Pharr analysis [11]. The AFM image of the indentation in Fig. 2 (f) shows no pile up which makes Oliver and Pharr method suitable for estimating the hardness and elastic modulus. The hardness and elastic modulus values obtained above and below 25 mN have shown a slight difference. The hardness of silicon loaded below 25 mN is in the range of 10-10.3 GPa and when loaded above 25 mN the hardness values obtained were in the range of 12-13 GPa. Similarly a change in elastic modulus is also observed above and below the load of 25 mN. Elastic modulus of silicon is found to vary in the range from 160-165 GPa for loading conditions below 25 mN whereas above 25 mN it is found to vary between 135-150 GPa. This variation of hardness and elastic modulus values with indentation load is shown in Fig. 3. The above observations indicate that 25mN (contact pressure of 11 GPa) is a critical load or pressure at which p-doped <100> silicon shows a transition in mechanical behaviour. The transition in mechanical behaviour has been attributed to pressure induced phase transformation [8] which silicon undergoes during indentation. It is this transformation which is responsible for variation in the shape of the unloading portion of the load-displacement curves. During indentation, the material in the sample directly beneath the rigid diamond indenter experiences very intense localized stresses and strains. In a small number of semiconductors and ceramic materials, these high stresses can cause plastic deformation not only by dislocation activity, but also by pressure-induced phase transformations to denser crystalline and amorphous forms [13-16]. It is well known that silicon transforms from the diamond cubic structure (dc) denoted Si-I to the metallic β-tin structure (Si-II) at a hydrostatic pressure in the range 11–13 GPa. On release of the pressure, the material first reverts to Si-XII (r8) and then to Si-III (bc8)

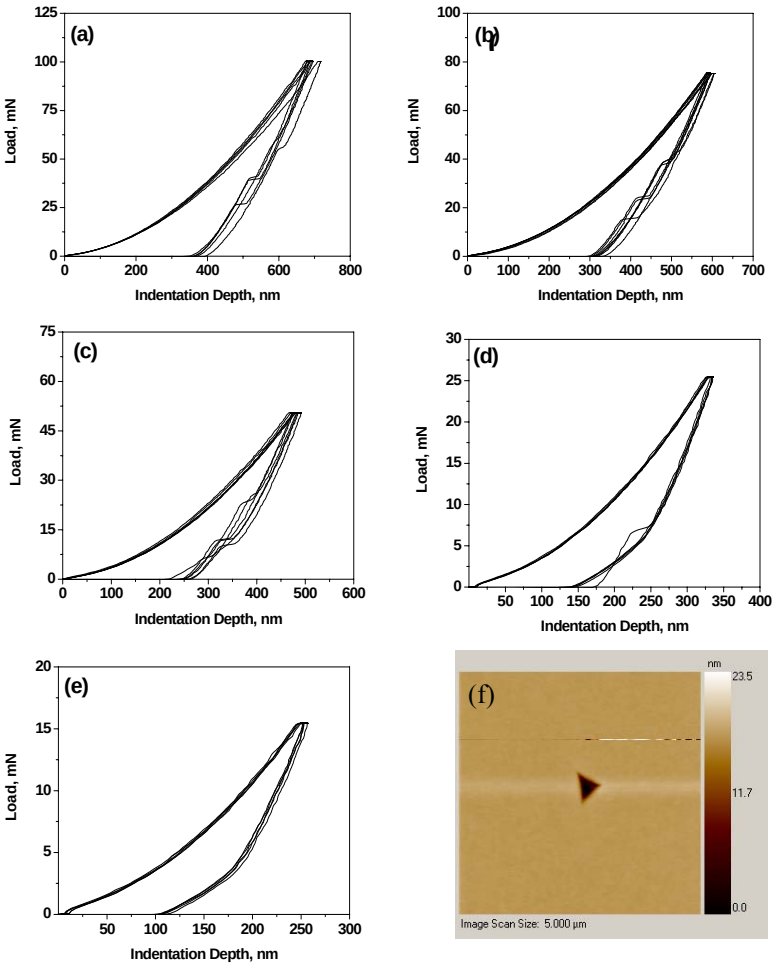

Fig. 2. Load-indentation depth curves for various loads from nanoindentation (a) 100 mN (b) 75 mN (c) 50 mN (d) 25 mN (e) 15 mN (f) AFM image of the residual indent at 50 mN.

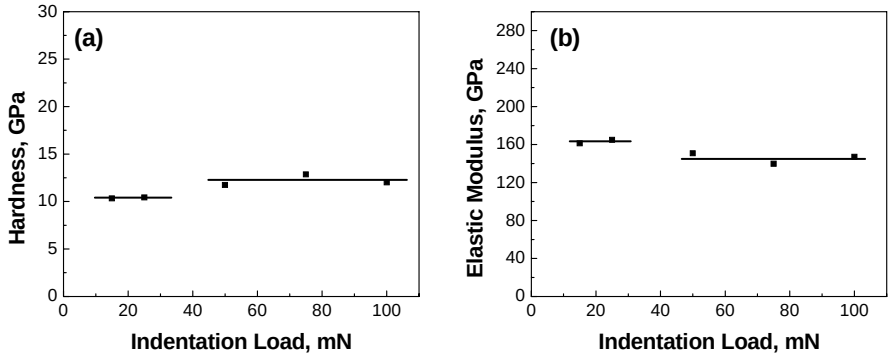

Fig. 3. Variation of (a) Hardness and (b) Elastic Modulus with the indentation load.

[17,18,19]. Gridneva et al. [20] and then Gerk and Tabor [21] suggested that the transformation from Si-I to Si-II also occurs during indentation, and that it may play an important role in determining the hardness of the material. Kailer et al. [22] also observed the metastable Si-XII/Si-III crystalline phases and an amorphous phase after indentation using micro-Raman techniques. They argued that the high-pressure Si-II phase transforms to the amorphous state during rapid unloading, whereas the crystalline phases form upon a slow load release.

Gogotsi and co-workers [23–26] suggested based on post-indentation micro-Raman studies that there is a good correlation between the unloading curve shape and the final structure of the transformed material. They proposed that the unloading discontinuity, often called the pop-out, corresponds to the formation of metastable Si-XII/Si-III crystalline phases, while the elbow in unloading, is associated with the formation of amorphous Si (a-Si). They also reported that higher maximum loads lead to pop-out while lower loads produce the elbow [23–26] which is also consistent with our observations. With decreasing load, the crystalline phases diminish and the amorphous phase becomes stronger.

It has also been reported that high indentation loading/unloading rates promote transition to amorphous phase [27]. To verify the above statement indentation experiments were done at different loading rates ranging from 25 mN/min to 300 mN/min at a load of 75 mN. There was no significant variation in the nature of the load versus indentation depth plots with loading rate and pop-out occurred in all cases. The hardness and elastic modulus values were also not found to vary significantly with loading rate in the loading rate range from 25 mN/min to 300 mN/min as shown in Fig. 4. The hardness was found to vary only between 12-12.5 GPa and the elastic modulus was found to vary between 128-134 GPa.

These results indicate that MEMS designers have to be careful when using silicon as cantilevers. They have to ensure that the contact pressure on silicon is always less than 11 GPa so that there is no change in the mechanical properties or the semiconducting properties of silicon.

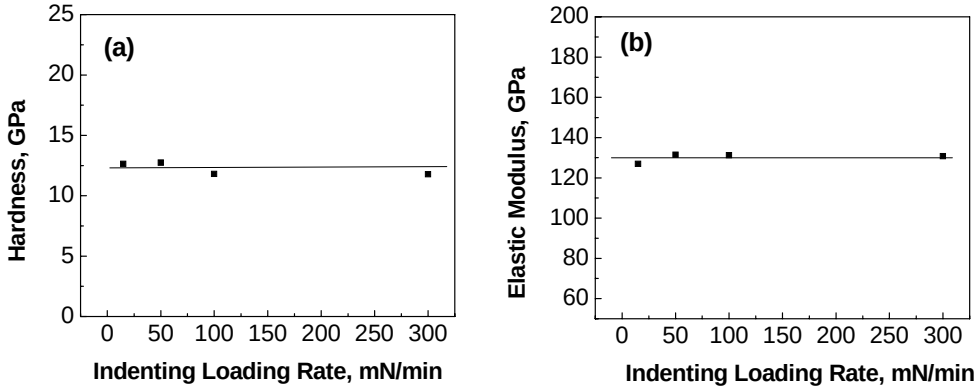

Fig. 4. Variation of (a) Hardness and (b) Elastic Modulus with loading /unloading rate.

3. 2. Silica

The load-indentation depth curves for silica film on silicon substrate for various loads are shown in Fig. 5. The AFM image of the indentation and its profile is shown in Figs. 6 (a) and (b), respectively. It is observed from the profile that there is no pile up around the indentation which makes Oliver and Pharr method [11] suitable for estimating the hardness and elastic modulus. It is observed that the values of hardness and elastic modulus do not show significant variation with respect to the increasing indentation depth. The hardness obtained is in the range of 10.5-11 GPa while the elastic modulus is found to vary between 84-87 GPa. These values are higher than those reported in the literature for bulk silica which again emphasize the importance of measurement of mechanical properties at the same length scale as that used in the MEMS device.

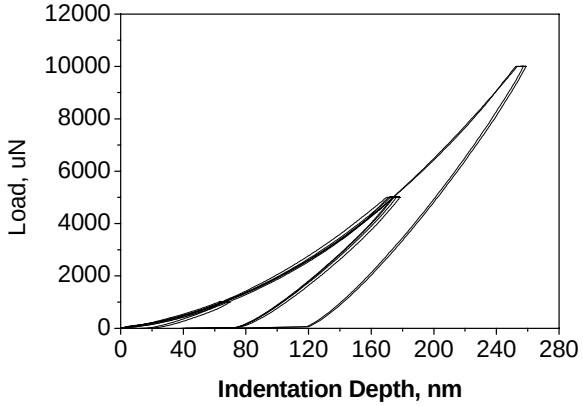

Fig. 5. Load-indentation depth curves for silica film on silicon substrate at various loads

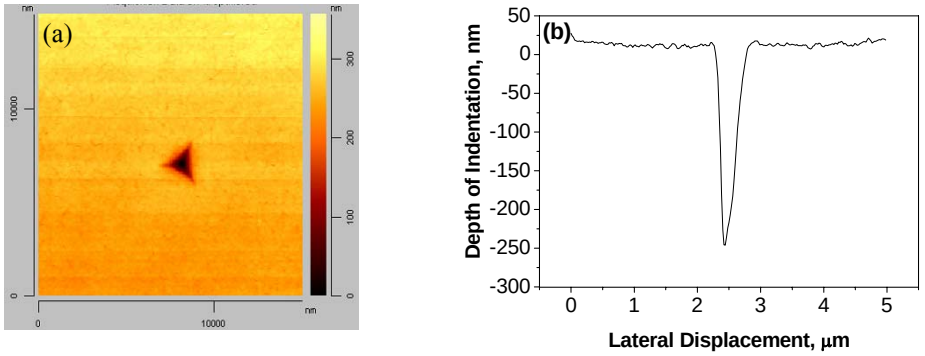

Fig. 6. (a) AFM Image of nanoindentation on silica film. (b) Depth profile of the indentation on silica

4. SUMMARY

The nanoindentation studies on p-doped <100> silicon have revealed that phase transformations and microstructural changes occur beneath the indenter. This is manifested in the load-indentation depth curve in the form of a pop-out and elbow. Higher indentation load were found to show pop-outs which indicated formation of metastable Si-XII/Si-III crystalline phases. On the other hand, low load indentations were found to show an elbow in the curve which indicated formation of amorphous phase. The mechanical properties of p-doped <100> silicon were found to be different above and below the critical load or contact pressure. The loading rate in the range of 25-300 mN/min was not found to influence the nature of the load versus indentation depth plots and pop-out occurred in all cases at a maximum load of 75 mN. The hardness and elastic modulus was also not found to vary with the loading rate. The hardness and elastic modulus of thermally grown silica film were found to be 10.5-11 GPa and 84-87 GPa which is higher than that reported in the literature for bulk silica.

ACKNOWLEDGEMENTS

The authors thank DRDO for providing funding to carry out this work. The authors also thank Shri V.K. Saravanan and Shri R. Singh, SSPL for help with sample preparation.

REFERENCES

[1] W. G. Knauss, I. Chasiotis, Y. Huang, *Mech. Mat.,* 35, 217-225 (2003).
[2] D. A. Lavan, B. L. Boyce,T. E. Buchheit, *Int. J. Dam. Mech*., 12, 357-362 (2003).
[3] H. Huang, F. Spaepen, *Acta Mater.,* 48, 3261-3269 (2000).
[4] N. Pugno 1, B. Peng, H.D. Espinosa, *Int. J. Sol. Struct*., 42, 647-661 (2005).
[5] Taechung Yi, Chang-Jin Kim, *Meas. Sci. Technol.* 10, 706–716 (1999).
[6] K. J. Hemker, H. Last, Mat. Sci.Engg. A, 319-321, 882-886 (2001).
[7] Brotzen, *Int. Mater. Rev*., 39,24-45 (1994).
[8] B. Bhusan and X. Li, *Int. Mater. Rev.*, 48, 125-164 (2003).
[9] X. Li, D. Diao, B. Bhusan, *Acta Mater*., 45, 4453-4457 (1997).
[10] B. Bhushan, X. Li, *J. Mater. Res.*, 12, 54-63 (1997).
[11] W. C. Oliver, G. M. Pharr*, J. Mater. Res.,* 7, 1564-1583 (1992).
[12] *ASM International Metals Handbook*, vol. 2, 889 (1990).
[13] V. Domnich, Y. Gogotsi In: Halwa HS, editor. Handbook of surfaces and interfaces of materials, vol. 2. New York: Academic Press; 2001. p.195.
[14] J. J. Gilman , *J. Mater. Res.*, 7, 535-538 (1992)
[15] M. Schmucker, H. Schneider, W. M. Kriven, *J. Am. Ceram. Soc.,* 86, 1821-1822 (2003)
[16] D. Ge , V. Domnich, T. Juliano, E. A. Stach, Y. Gogotsi., *Acta Mater.,* 52, 3921-3927 (2004).
[17] J. Z. Hu, L. D. Merkle, C. S. Menoni, I. L. Spain, *Phys. Rev. B,* 34, 4679-4686 (1986).
[18] J. Crain, G. J. Ackland, J. R. Maclean, R. O. Piltz, P. D. Hatton, G. S. Pawley, *Phys. Rev. B,* 50, 13043 (1994).
[19] R. O. Piltz, J. R. Maclean, S. J. Clark, G. J. Ackland, P. D. Hatton, J. Crain, *Phys. Rev. B,* 52, 4072-4078 (1995)
[20] V. Gridneva, Y. V. Milman, V. I. Trefilov, *Phys. Stat. Sol.,* 9, 177-184 (1972).
[21] A. P. Gerk, D. Tabor, *Nature,* 271, 732-739 (1978).
[22] A. Kailer, Y. Gogotsi, K. G. Nickel, *J. Appl Phys.,* 81, 3057-3062 (1997).
[23] V. Domnich, Y. Gogotsi, S. Dub, *Appl. Phys. Lett.,* 76, 2214-2219 (2000).
[24] Y. Gogotsi, V. Domnich, S. Dub. *J. Mater. Res.,* 15, 871-879 (2000).
[25] T. Juliano, Y. Gogotsi, V. Domnich, *J. Mater. Res*., 18, 1192-1201 (2003).
[26] V. Domnich, Y. Gogotsi, *Rev Adv Mater Sci.,* 3, 1-6 (2002).
[27] Jae-il Jang, M. J. Lance, S. Wen, T. Y. Tsui, G. M. Pharr, *Acta Mater.,* 53, 1759-1770 (2005).